Structural Dynamics of Rotating Bladed-Disk Assemblies Coupled with Flexible Shaft Motions

R. G. Loewy* and N. Khader†
Rensselaer Polytechnic Institute, Troy, New York

A classical structural dynamics approach is used to couple the motion of a flexible bladed disk typical of modern aircraft turbines to a rotating, flexible shaft. Transformations between fixed and rotating coordinate systems, Lagrange's equations, and routine manipulation lead to a system of second-order differential equations with constant coefficients. Flexible disk displacements transverse to the plane of rotation and radial and tangential as well are accounted for. Rigid disk translations along, and rotations about, axes normal to the undeformed shaft axes are also included. Displacements of the flexible bladed-disk assembly are expressed in terms of the nonrotating mode shapes obtained from finite element analysis with the disk hub fixed in space and associated with their time-dependent generalized coordinates. The resulting eigenvalue problem for the coupled, rotating natural modes and frequencies is of small size and easily solved by available computer subroutines. Using this method, the Pratt & Whitney first-stage compressor/fan of the "E^3" engine has been analyzed for a wide range of shaft flexibilities and shaft speeds. Some of the one-diametral node frequencies are shown to be affected significantly by shaft degrees of freedom with stiffness values in the general range of design practice. Coriolis forces are also shown to affect natural frequencies appreciably where there is strong coupling between certain modes.

I. Introduction

IT is important to be able to predict the natural frequencies of turbomachinery parts under operating conditions during the design stage. In that respect, the problem is similar to proper structural dynamic design of fixed-wing aircraft lifting surfaces, propeller and rotor blades, and other high-performance structures. For turbomachinery bladed-disk assemblies, however, the problem is especially challenging because the costs of the developments are high, the rotational speeds are high, the aspect ratios of the blade are low and their geometry complex in other respects, and weight considerations are stringent enough that the parts are highly stressed. In fact, even in some of the most recent engine developments, inability to accurately predict proximity of a natural mode to resonance with an integer harmonic force had a significant effect on the fatigue life of certain compressor stages.

The increasing degree of sophistication of analyses devised to deal with the problem is seen clearly in the literature. In some of the earlier works, turbomachinery blades were modeled as is done for helicopter or propeller blades, i.e., as simple beams.[1-9] Plate and shell theories were later applied in attempts to better account for the low aspect ratios typical of such parts.[10-12] The advent of finite element methods (FEM) held great promise for turbomachinery analysis, as it had for so many other fields, and applications were not long in coming.[13-20] The special configurational aspects of bladed disks are also recognized in the literature—in analyses coupling the motion of one blade to another through "shrouds," and through disk motion.[21-30] The useful concepts growing out of polar symmetry also have been combined with FEM so that natural frequencies and mode shapes of an entire assembly can be obtained from the analysis of a single blade with its associated portion (or segment) of the disk by properly selecting boundary conditions along the borders of the disk segment.[31,32]

With all of this analytical effort, the complexity of the problem has been such as to cause some potentially significant aspects to remain incompletely investigated or ignored altogether. Among these is a full representation of the rotational dynamics. Most FEM applied to rotating structures include only centrifugal stiffening. Coriolis forces are incorporated in very few analyses of any kind; one specific investigation is that of Sisto.[33,34] Furthermore, flexible shaft phenomena have been dealt with by assuming almost exclusively that bladed-disk assemblies ae rigid, and all of the previously mentioned studies of flexible bladed disks have assumed rigid shafts and bearings. It should be noted that phenomena in which flexible or hinged helicopter rotor blades and propellers have coupled, often disastrously, with motions of flexibly mounted hubs are well known in those industries.[35-38]

This paper investigates the importance of such effects, including full rotational dynamics for small-perturbation motions about some very general initial configurations and, particularly, the effect of flexible shaft motion on the natural modes and frequencies of polar symmetric, bladed-disk assemblies.

II. Analytical Approach

In the method chosen for this analysis, we assumed that natural modes and frequencies of the nonrotating bladed-disk assembly with its hub rigidly supported are known in detail from either shake test or FEM analysis. These modes and the flexible shaft motions are used as generalized coordinates in a classical small-perturbation Lagrangian formulation. Thus the structural complexity of the problem is relegated to a preliminary single analysis or test in which (except for steady deformations associated with centrifugal force) all rotational dynamics are eliminated. The rotational dynamics are then represented in the subject analysis, in which the structural aspects have been eliminated. In fact, the number of degrees of freedom is limited to those of the shaft plus two times the

Presented as Paper 83-0919 at the AIAA/ASME/ASCE/AHS 24th Structures, Structural Dynamics and Materials Conference, Lake Tahoe, Nev., May 2-4, 1983; submitted June 2, 1983; revision received Oct. 28, 1983.

*Institute Professor. Fellow AIAA.
†Postdoctoral Research Fellow.

number of nonrotating, rigid hub modes that are included, as explained in Sec. II.A.

A. Flexible Motion of the Bladed-Disk Assembly

The small oscillatory motion of a point on the bladed-disk assembly, with respect to its hub in a coordinate system at a particular azimuth location and rotating with the disk, is expressed in the general form

$$\bar{w}(x,y,z,t) = \sum_{n}^{2b} q_n(t)\,\bar{w}_n(x,y,z)$$

where $\bar{w}$ is the deflection of the point at x,y,z with respect to the hub; $\bar{w}_n$ the deflection of that point with respect to the hub in the nth (normalized) nonrotating, rigid shaft mode shape; q_n the generalized coordinate for that nth natural mode; b the total number of such modes used; and barred quantities denote vectors or matrices.

It is noted here that for a bladed-disk assembly with polar symmetry, only modes with one diametral node line will couple with shaft motion. Accordingly, only such modes will be considered in this analysis. On the other hand, it is not known, a priori, where the node line will fall with respect to flexible shaft motions, or if and how it will move as a traveling wave. Thus each normal mode of the flexible bladed-disk assembly must be used twice. It is convenient to place their node lines at 90 deg to each other, azimuthally. Each has its own distinct generalized coordinate, q_n. Thus motions on the bladed disk are actually expressed as

$$\bar{w}(x,y,z,t) = \sum_{n}^{b} \left[q_c^{(n)}(t)\,\bar{w}_c^{(n)}(x,y,z) + q_s^{(n)}(t)\,\bar{w}_s^{(n)}(x,y,z)\right] \tag{1}$$

B. Flexible Shaft Motion

Motions of the hub due to shaft (or bearing) flexibility are expressed in a nonrotating system of axes fixed in space. Four degrees of freedom are accounted for; linear translations in two directions and angular rotations in two directions, all with respect to axes perpendicular to the undeflected shaft axis and each other.

These motions and the forces and moments which must be applied (at the point of attachment of hub to shaft) in order to cause them, are related by the appropriate stiffness matrix coefficients. (Taken here in terms of a uniform cantilever shaft of length ℓ and polar symmetric bending rigidity, EI.)

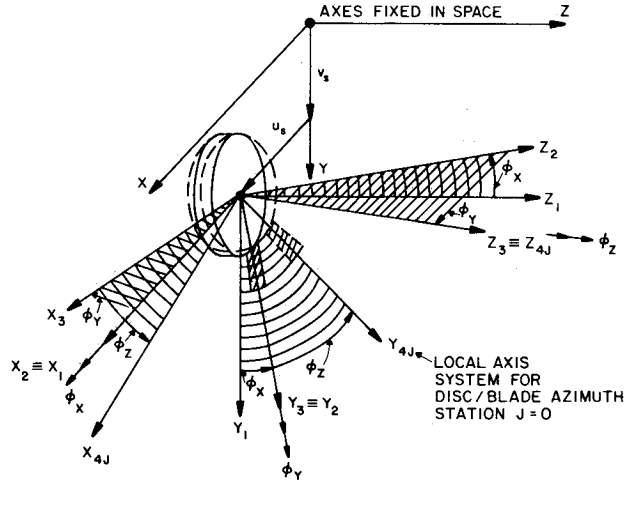

Fig. 1 Transformation from axes fixed in space to disk/blade system at azimuth station $J=0$.

$$\begin{vmatrix} F_x \\ M_y \\ F_y \\ M_x \end{vmatrix} = \frac{EI}{\ell^3} \left[\begin{array}{cc:cc} 12 & -6\ell & & \\ -6\ell & 4\ell^2 & \multicolumn{2}{c}{[0]} \\ \hdashline & & 12 & 6\ell \\ \multicolumn{2}{c:}{[0]} & 6\ell & 4\ell^2 \end{array}\right] \begin{vmatrix} u_s \\ \phi_y \\ v_s \\ \phi_x \end{vmatrix} \tag{2}$$

The motions of the flexible bladed-disk assembly [Eq. (1)] can be related to those of the shaft by expressing them in the same fixed-in-space axis system. This is done through the successive transformations written below as Eq. (3) and illustrated in Fig. 1.

$$\begin{vmatrix} X \\ Y \\ Z \end{vmatrix} = \begin{vmatrix} x \\ y \\ z \end{vmatrix}_1 + \begin{vmatrix} u_s \\ v_s \\ 0 \end{vmatrix}$$

$$\begin{vmatrix} x \\ y \\ z \end{vmatrix}_1 = \begin{bmatrix} 1 & 0 & 0 \\ 0 & \cos\phi_x & -\sin\phi_x \\ 0 & \sin\phi_x & \cos\phi_x \end{bmatrix} \begin{vmatrix} x \\ y \\ z \end{vmatrix}_2 \triangleq \bar{\phi}_x \begin{vmatrix} x \\ y \\ z \end{vmatrix}_2$$

$$\begin{vmatrix} x \\ y \\ z \end{vmatrix}_2 = \begin{bmatrix} \cos\phi_y & 0 & \sin\phi_y \\ 0 & 1 & 0 \\ -\sin\phi_y & 0 & \cos\phi_y \end{bmatrix} \begin{vmatrix} x \\ y \\ z \end{vmatrix}_3 \triangleq \bar{\phi}_y \begin{vmatrix} x \\ y \\ z \end{vmatrix}_3$$

$$\begin{vmatrix} x \\ y \\ z \end{vmatrix}_3 = \begin{bmatrix} \cos\phi_{zj} & -\sin\phi_{zj} & 0 \\ \sin\phi_{zj} & \cos\phi_{zj} & 0 \\ 0 & 0 & 1 \end{bmatrix} \begin{vmatrix} x \\ y \\ z \end{vmatrix}_{4j} \triangleq \bar{\phi}_{zj} \begin{vmatrix} x \\ y \\ z \end{vmatrix}_{4j}$$

where

$$\phi_{zj} = \frac{2\pi}{N}(j-1) + \Omega t \qquad j = 1,2,\ldots,N$$

i.e., a particular azimuthal segment.

Adding the subscript k to differentiate one point within the jth azimuthal disk segment and blade from another, then

$$\begin{vmatrix} x \\ y \\ z \end{vmatrix}_{4jk} = \begin{vmatrix} Q_1 \\ Q_2 \\ Q_3 \end{vmatrix}_{jk} + \bar{w}_{jk}$$

$$\triangleq \{Q\}_{jk} = \begin{vmatrix} Q_1 + \sum_{n=1}^{b} \left[q_n^{(c)}(t)\,u_n^{(c)} + q_n^{(s)}(t)\,u_n^{(s)}\right] \\ Q_2 + \sum_{n=1}^{b} \left[q_n^{(c)}(t)\,v_n^{(c)} + q_n^{(s)}(t)\,v_n^{(s)}\right] \\ Q_3 + \sum_{n=1}^{b} \left[q_n^{(c)}(t)\,w_n^{(c)} + q_n^{(s)}(t)\,w_n^{(s)}\right] \end{vmatrix}_{jk}$$

Here, Q_1, Q_2, and Q_3 are vector components of the steady, equilibrium position of the jth mass point. Hence,

$$\bar{X}_{jk} \triangleq \begin{vmatrix} X \\ Y \\ Z \end{vmatrix}_{jk} = \begin{vmatrix} u_s \\ v_s \\ 0 \end{vmatrix} + \{A\}_{jk} \tag{3}$$

where

$$\{A\}_{jk} \triangleq \bar{\phi}_x \bar{\phi}_y \bar{\phi}_{zj} \{Q\}_{jk}$$

Here $\bar{X}_{jk}$ are the coordinates of the kth mass point within the jth azimuthal segment of the bladed-disk assembly, as expressed in the fixed-axis system. The subscript *1*, attached to the column matrix, denotes the shaft center axis system, nonrotating, untilted, but translated; subscripts *2* and *3* on the column matrices denote the nonrotating shaft center-axis systems, translated and tilted first in one direction and then both directions normal to the shaft centerline; subscript *4* denotes the coordinate system of Eq. (1), i.e., at a particular azimuthal location and rotating with the bladed disk.

C. Equations of Motion

With the expressions it is now a matter of some labor, but routine, to write an expression for the kinetic energy of the system

$$T = \sum_{j=1}^{\alpha} \sum_{k=1}^{\beta} (m\dot{\bar{X}}^T \dot{\bar{X}})_{jk} = T(q_i \dot{q}_i) \tag{4}$$

where α is the number of azimuthal sections, usually chosen as equal to the number of blades; β the number of mass points m within the jth azimuthal sector, located at various radial and chordwise positions on the blades, or similarly on the disk. (Shaft mass may be represented as "lumped" with the innermost disk masses.) Superscript T denotes the matrix transpose and i is used here, rather than n, as in Eq. (1), to indicate that q_i includes the flexible shaft coordinates u_s, v_s, ϕ_x, and ϕ_y, as well as all the bladed-disk modes thought of as associated with q_n.

Lagrange's equations are now dealt with in the following form:

$$\underbrace{\frac{\mathrm{d}}{\mathrm{d}t}\left(\frac{\partial T}{\partial \dot{q}_i}\right) - \frac{\partial T}{\partial q_i} + \frac{\partial U}{\partial q_i}}_{-(Q_i) \quad +(Q_i)} = Q_i \tag{5}$$

inertia forces; restoring forces; generalized force in the ith normal mode

and for the free vibrations case, of course, $Q_i \equiv 0$. Equation (3), substituted into Eq. (5), leads to nonlinear expressions for inertia forces in a form shown in Eq. (6).

$$-(Q_i)_{\text{inertia}} = a_{ij}\ddot{q}_j + \Omega(a_{ij,\psi} + a_{\psi i,j} - a_{\psi j,i})\dot{q}_j + \Omega^2(a_{\psi i,\psi} - \tfrac{1}{2}a_{\psi\psi,i}) + (a_{ij,k} - \tfrac{1}{2}a_{jk,i})\dot{q}_j\dot{q}_k \tag{6}$$

Here the coefficients a_{ij} are lengthy expressions involving the masses, coordinates of position, the natural modes shapes, and the generalized coordinates. The rotational variable ψ, however, will disappear, thanks to the properties of the orthogonal transformations shown in Eq. (3). The subscripts following commas indicate partial derivatives with respect to the generalized coordinates and the rotational variable ψ.

These equations, linearized by expanding in a Taylor series about the equilibrium position and truncating second- and higher-order terms in the generalized coordinates, yield Eq. (7), in which the zero subscript indicates steady, equilibrium quantities.

$$-(Q_i)_{\text{inertia}} \cong (a_{ij})_0\ddot{q}_j + \Omega(a_{ij,\psi} + a_{\psi i,j} - a_{\psi j,i})_0\dot{q}_j + \Omega^2(a_{\psi i,\psi j} - \tfrac{1}{2}a_{\psi\psi,ij})_0 q_j + \Omega^2(a_{\psi i,\psi} - \tfrac{1}{2}a_{\psi\psi,i})_0 \tag{7}$$

The potential energy U consists of three parts: 1) that due to elastic energy in the nth nonrotating, hub-fixed natural mode of the bladed disk $\triangleq U_{1n}$; 2) that due to shaft bending $\triangleq U_2$; and 3) that produced by centrifugal forces acting through those displacements in all the natural modes in the radial direction such as are caused by bending and twisting of elements which are radially inextensible $\triangleq U_3$ (see, for example, Ref. 39).

The total potential energy is thus (using the q_n and $2b$ notations, rather than $q_n^{(c)}$, $q_n^{(s)}$, and b, for simplicity):

$$U = \sum_{n}^{2b} U_{1n} + U_2 + U_3 \tag{8}$$

where

$$U_{1n} = \tfrac{1}{2}k_{\text{eff}_n} q_n^2 \tag{8a}$$

$$U_2 = \left(\frac{EI}{2\ell^3}\right) \overline{u_s \phi_y \mid v_s \phi_x} \left[\begin{array}{cc|cc} 12 & -6\ell & & \\ -6\ell & 4\ell^2 & \multicolumn{2}{c}{[0]} \\ \hline & & 12 & 6\ell \\ \multicolumn{2}{c|}{[0]} & 6\ell & 4\ell^2 \end{array}\right] \left|\begin{array}{c} u_s \\ \phi_y \\ v_s \\ \phi_x \end{array}\right| \tag{8b}$$

$$U_3 = \frac{1}{2}\Omega^2 \sum_{j=1}^{N} \sum_{t=1}^{T} \sum_{r=1}^{R} \left[Q_2 \left(m \int_{y_0}^{Q_2} \left[\left(\frac{\partial w}{\partial y}\right)^2 + \left(\frac{\partial u}{\partial y}\right)^2 \right] \mathrm{d}y \right) + Q_1 \left(m \int_{x_0}^{Q_1} \left[\left(\frac{\partial w}{\partial x}\right)^2 + \left(\frac{\partial v}{\partial x}\right)^2 \right] \mathrm{d}x \right)_{tr} \right]_j \tag{8c}$$

where subscripts r and t indicate values of the masses formerly identified by the subscript k, grouped to indicate summation along the radial direction at a particular tangential strip (i.e., at a fixed chord location) as indicated by rt; and vice versa, as indicated by tr; u, v and w are chordwise, radial, and transverse components, respectively, of the displacements given by Eq. (1). R and T are the numbers of radial and tangential beams, as shown in Fig. 2, and N is the number of blades in the bladed-disk assembly.

Performing the operations on potential energy to obtain restoring forces and adding them to the inertia terms as indicated in Eq. (5) leads to a system of simultaneous, linear, second-order differential equations in the generalized coordinates whose terms resulting from flexible shaft motions have periodic coefficients. These equations of motion can be put in final form by defining a new set of coordinates

$$Q_1^{(n)} \triangleq q_n^{(s)} \sin\Omega t + q_n^{(c)} \cos\Omega t$$
$$Q_2^{(n)} \triangleq q_n^{(s)} \cos\Omega t - q_n^{(c)} \sin\Omega t \tag{9}$$

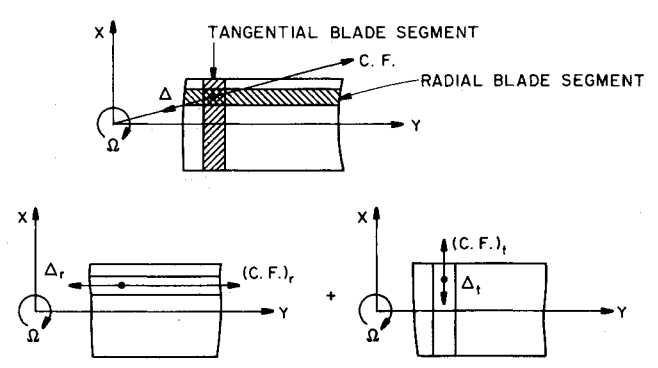

Fig. 2 Equivalent beam representation of the blade by segments.

which will be recognized as the flexible bladed-disk coordinates as seen in a fixed-in-space coordinate system. Then, by properly manipulating our equations with periodic coefficients, one obtains a final set of equations of motion, all of whose terms have constant coefficients. Expressed in matrix notation, it has the classical form,

$$[\bar{M}]\{\ddot{\bar{q}}\}+[\bar{C}]\{\dot{\bar{q}}\}+[\bar{K}]\{\bar{q}\}=0 \qquad (10)$$

The full set of equations, whose complete derivation is presented in Ref. 40, is given in the Appendix.

D. Solution for Rotating Natural Frequencies and Mode Shapes

Equation (10) is solved by assuming a solution of general form $q_i=q_{i0}e^{\lambda t}$ where both q_{i0} and λ are complex. Substitution into the differential equation results in an eigenproblem solution for the eigenvalues λ_r and the eigenvectors $q_{i0}^{(r)}$. Values of λ_r in conjugate imaginary pairs denote natural frequencies. Since damping has not been considered, no negative real parts would be expected in the solution for λ_r; a positive real part would signify a mechanical instability.

E. Results of Numerical Examples

To examine the efficiency of the method and the importance of the new effects in a practical example, an actual turbofan engine first-stage compressor fan disk was analyzed. The Pratt & Whitney "E^3" engine was chosen by NASA Lewis Research Center and the mass, geometry, and nonrotating, fixed-hub natural modes and frequencies for this compressor fan were provided by Pratt & Whitney of Hartford, Conn. This fan has 24 blades, and the finite element analysis performed at Pratt & Whitney to calculate the nonrotating modes and frequencies had 665 masses, each with from 3 to 6 degrees of freedom, in each of the 24 segments. Shaft stiffness information in a form compatible with Eq. (2) was also made available along with operational rpm data.

The first steps taken were to assess the adequacy of the mathematical model. Accordingly, hub-fixed rotating modes were calculated using varying numbers of nonrotating modes and increasing numbers of radial and chordwise breakdowns for the centrifugal stiffening calculation [see Eq. (8c) and Fig. 2]. These studies parallel earlier investigations on a helicopter blade, reported in Ref. 41. The results are similar. As shown in Fig. 3, representation of centrifugal stiffening by 40 tangential and 20 radial beams would certainly appear to be adequate for up to four flexible, bladed-disk modes. Similarly, use of three nonrotating mode shapes seems sufficient to the task of predicting the first two flexible rotating natural frequencies (Fig. 4).

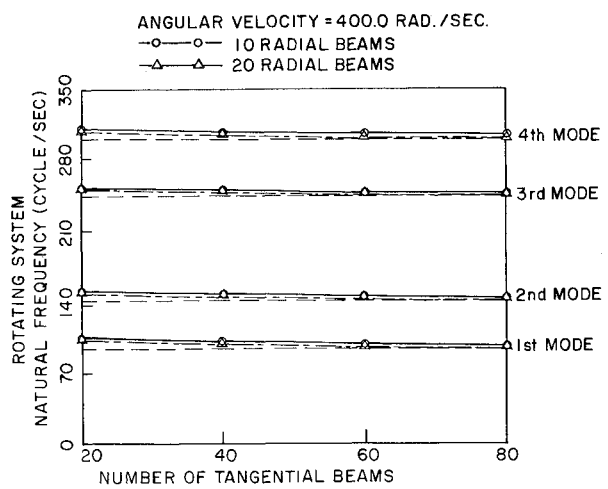

Fig. 3 Effect of the number of tangential and radial beams used to account for centrifugal stiffening on fixed-hub, rotating natural frequencies (see Fig. 2).

The effects of shaft flexibility are complicated enough to suggest a step by step exposition. Figure 5 shows on one plot, uncoupled modes of two kinds. The horizontal lines represent four, one-diametral node, flexible blade/disk modes with the hub fixed. The curved lines show the natural frequencies of translating and tilting rigid blade/disks on shafting of continuously variable flexibility. All modes in Fig. 5 are at $\Omega=0$. Figure 6 is a reiteration of Fig. 5, but for the rotational case where $\Omega=400$ rad/s. In this case each fixed-hub, flexible bladed-disk mode appears twice because it is viewed in the fixed system (i.e., $w_n=w_{n\ \text{rotating}}\pm\Omega$), and each mode of the rigid disk on the flexible shaft "splits" into forward whirl (progressive) and backward whirl (retrogressive) modes.

Figure 7 shows the $\Omega=0$ condition, again, but now the solid curves indicate the effect of coupling one bladed disk mode and two shaft modes. Figure 8 repeats Fig. 7 but, in this case, at $\Omega=400$ rad/s. "Splitting" of modes into progressive and regressive whirl cases now changes the coupling between blade/disk and shaft modes, so that the disk modes viewed in the fixed system can no longer be expected, in general, to differ by $\pm\Omega$, even when only one blade/disk mode is involved. Dashed lines are included to show the uncoupled frequencies, and the comparison shows that even for very stiff shafts significant differences in disk frequencies can be expected. Some mention should be made here regarding the fact that the frequencies of the disk modes (solid line) at a very high shaft stiffness are not the same as those calculated for rigid shaft modes (dashed line). This difference, seen in Figs. 7-9, exists because the solid line modes were calculated using only one disk mode, while the dashed line results were

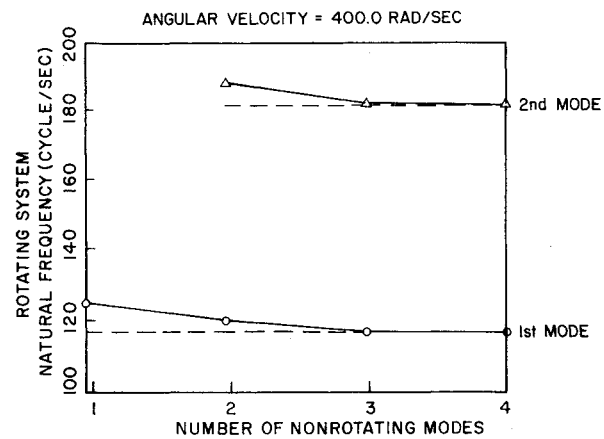

Fig. 4 Effect of the number of nonrotating disk modes used in the analysis as generalized coordinates on the fixed-hub, rotating natural frequencies.

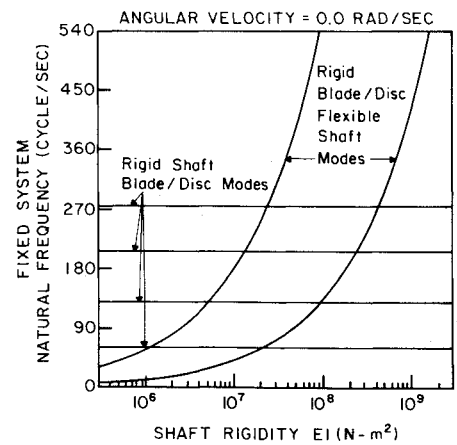

Fig. 5 Uncoupled frequencies vs shaft stiffness (shaft length, 88.9 cm) at angular velocity = 0, one flexible disk mode.

calculated using four disk modes. This is the same sort of difference shown in Fig. 4.

The matrix which multiplies the generalized velocities, $\dot{q}$, in Eq. (10) is due solely to gyroscopic and Coriolis forces. While some confusion often exists as to differentiating between the two, in this paper we understand the former to refer to terms associated with rigid rotating body motion and the latter to flexible rotating body motion. Figure 9 repeats the calculations of Fig. 8 but, as is often done, with the Coriolis terms neglected. Significant frequency differences due to neglecting Coriolis forces can be seen in the "cross-over" regions with the blade/disk regressive modes; elsewhere the effects seem negligible.

Figures 10-12 are basically the same as Figs. 7-9, respectively, but with four flexible bladed-disk modes used to produce the former figures, whereas, only one flexible disk mode was included in the calculation producing the latter group.

Figures 10-12 are more complicated. Careful examination, however, reveals the same facts observed in Figs. 7-9. For example,

1) Flexible bladed-disk modes are highly coupled to the rigid disk-flexible shaft modes for low or moderately high values of shaft stiffness.

2) For extremely high shaft stiffness, rigid disk modes uncouple from the flexible modes and, as one would expect, the latter approach modes which were calculated assuming a rigid shaft.

3) When the coupling between rigid and flexible modes is strong, frequencies corresponding to forward and backward disk modes seen in a fixed coordinate system are not separated by $\pm\Omega$ as is the case in rigid shaft analysis.

4) Frequency differences due to Coriolis effects are appreciable only in the cross-over regions.

Since a primary objective of structural dynamics analysis is to obtain an accurate estimate of the location of resonance points, a Campbell diagram of modes calculated using the

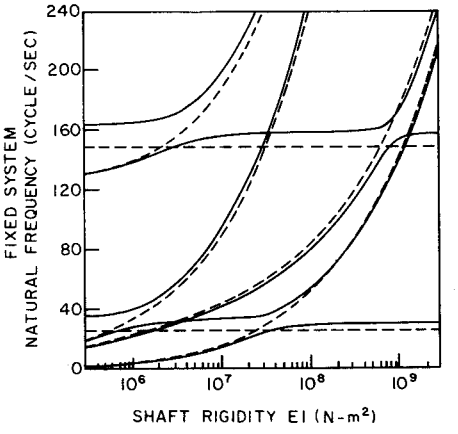

Fig. 8 Coupled and uncoupled frequencies vs shaft stiffness (shaft length, 88.9 cm) at angular velocity = 400 rad/s, one flexible disk mode.

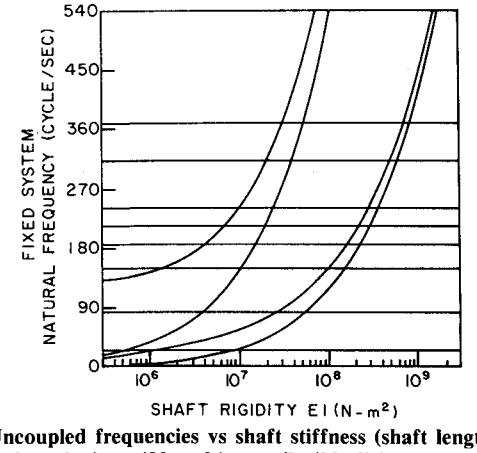

Fig. 6 Uncoupled frequencies vs shaft stiffness (shaft length, 88.9 cm) at angular velocity = 400, rad/s, one flexible disk mode.

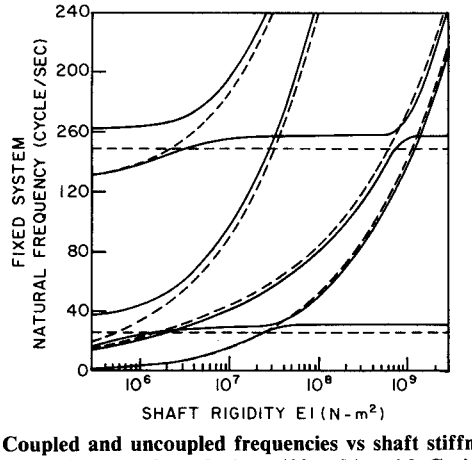

Fig. 9 Coupled and uncoupled frequencies vs shaft stiffness (shaft length, 88.9 cm) at angular velocity = 400 rad/s, with Coriolis forces neglected, one flexible disk mode.

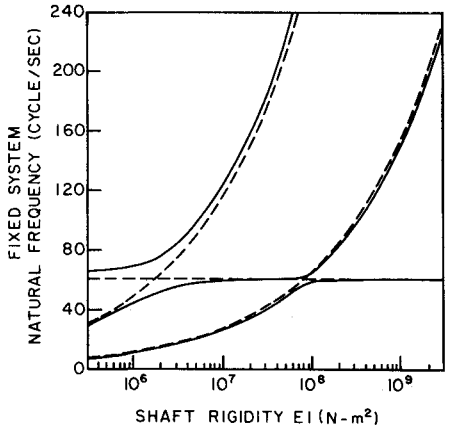

Fig. 7 Coupled and uncoupled frequencies vs shaft stiffness (shaft length, 88.9 cm) at angular velocity = 0, one flexible disk mode.

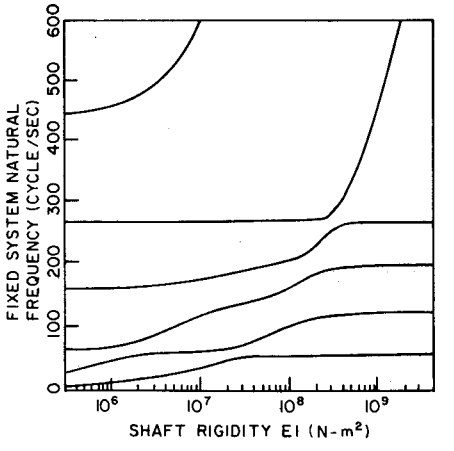

Fig. 10 Coupled frequency vs shaft stiffness (shaft length, 88.9 cm), at angular velocity = 0, four flexible disk modes.

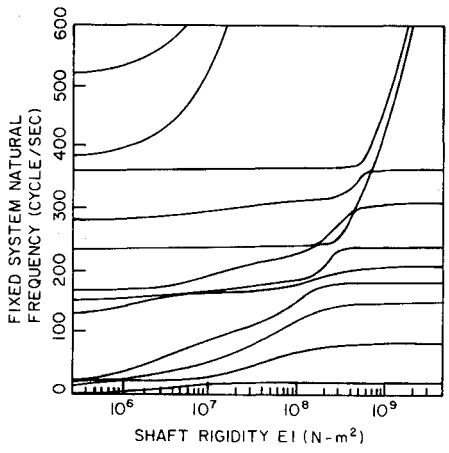

Fig. 11 Coupled frequency vs shaft stiffness (shaft length, 88.9 cm), at angular velocity = 400 rad/s, four flexible disk modes.

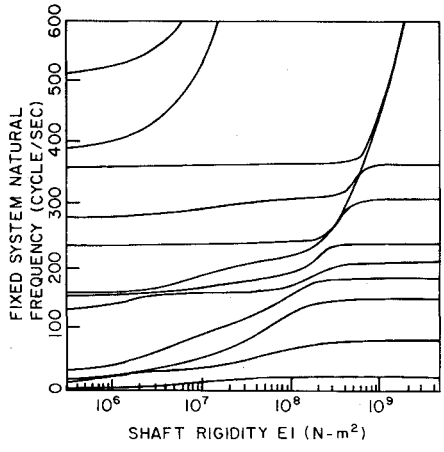

Fig. 12 Coupled frequency vs shaft stiffness (shaft length, 88.9 cm), at angular velocity = 400 rad/s, with Coriolis forces neglected, four flexible disk modes.

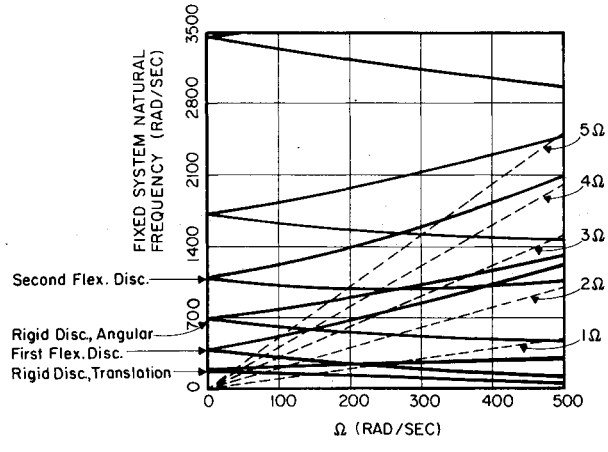

Fig. 13 Coupled frequency vs angular velocity Ω (shaft $EI = 5.60 \times 10^6$ N/m², length 88.9 cm).

subject method for the operating region (300-500 rad/s) is shown in Fig. 13. A similar plot for the same bladed disk uncoupled from the shaft (i.e., where flexible disk modes are on a rigid shaft and the flexible shaft modes are for a rigid bladed disk) is presented in Fig. 14. The nature of the modes in these figures is indicated on the ordinates of the zero rotational speed points. Such identification is aided by

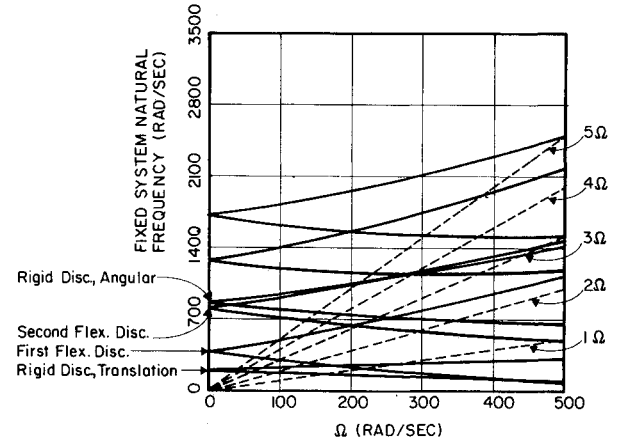

Fig. 14 Uncoupled frequency vs angular velocity Ω (rigid disk modes calculated for shaft $EI = 5.60 \times 10^6$ N/m² and length 88.9 cm, flexible disk modes calculated with a rigid shaft).

considering the variation of frequency with shaft stiffness in Figs. 10-12. Comparing resonance points from one case (figure) to the other shows how substantial the effect produced by shaft flexibility can be on the structural dynamics characteristics of flexible, rotating bladed disks. For example, without shaft flexibility (Fig. 14), the second flexible disk mode is in resonance with the first harmonic at Ω = 495 rad/s, the second harmonic at Ω = 300 rad/s, both in a retrogressive whirl, and the third harmonic at Ω = 480 rad/s, in a progressive whirl. When shaft flexibility is accounted for, we see from Fig. 13 that, the same second flexible disk mode is in retrogressive whirl resonance with the third harmonic at Ω = 330 rad/s and is in progressive whirl with the fifth harmonic at Ω = 340 rad/s. Its 1Ω retrogressive and 3Ω progressive resonances are well beyond 500 rad/s. Similar differences are seen when frequencies of other modes are compared for the analysis with and without shaft flexibility effects.

III. Conclusions

A set of linear, second-order differential equations with constant coefficients, governing the dynamic motion of a rotating flexible bladed-disk assembly on a flexible shaft has been formulated. The following conclusions are drawn as a result of calculations using a realistic, first-stage compressor-fan and variations in several important parameters: The Lagrangian approach used in the analysis is straightforward and allows an accounting of both disk motion due to shaft flexibility and Coriolis effects.

The number of nonrotating bladed-disk modes used with generalized coordinates to express the displacements in the rotating modes was small. It was shown that only four such modes are enough to obtain satisfactory results for the first three coupled modes. This allowed the equations of motion to be represented by an eigenvalue problem of low order. The computer time required to solve such problems is known to be proportional to the cube of the order of such systems. When four nonrotating modes are used, the order of the resulting system of equations presented here is 12. This can be compared with the hundreds or even thousands of degrees of freedom in a finite element analysis used directly in the dynamic calculation. Using the subject analysis, the lowest eight eigenvalues and associated eigenvectors were obtained for five different values of the angular velocity, for only 1.33 s of CPU time on an IBM 3033.

Although accounting for Coriolis forces introduces small changes in the resulting frequencies for the most part, in regions where rigid and flexible modes are highly coupled, these terms can have a substantial effect. Shaft flexibility has considerable influence on certain rotating coupled frequencies of flexible bladed-disk-shaft assemblies for values typically

used. This effect should be included in analyses to obtain accurate structural dynamics characteristics if one is to be certain of a reliable fan, compressor, or turbine design.

Appendix

The linearized equations of motion transformed into constant coefficient form are listed below.

$$F\ddot{u}_s + G\ddot{\phi}_y + \sum_{p=1}^{b} [-\eta_p^{(s)} \ddot{Q}_1^{(p)} + \xi_p^{(s)} \ddot{Q}_2^{(p)}] + k_{uv} u_s + k_{ux} \phi_y = 0$$

$$F\ddot{v}_s - G\ddot{\phi}_x + \sum_{p=1}^{b} [\xi_p^{(s)} \ddot{Q}_1^{(p)} + \eta_p^{(s)} \ddot{Q}_2^{(p)}] + k_{uv} v_s - k_{ux} \phi_x = 0$$

$$H\ddot{\phi}_x - G\ddot{v}_s + \sum_{p=1}^{b} [A_p^{(s)} \ddot{Q}_1^{(p)} + B_p^{(s)} \ddot{Q}_2^{(p)}] + 2\Omega\alpha\dot{\phi}_y + 2\Omega \sum_{p=1}^{b} [\gamma_p^{(s)} \dot{Q}_1^{(p)} - \delta_p^{(s)} \dot{Q}_2^{(p)}] - k_{ux} v_s + k_{xy} \phi_x = 0$$

$$H\ddot{\phi}_y + G\ddot{u}_s + \sum_{p=1}^{b} [B_p^{(s)} \ddot{Q}_1^{(p)} - A_p^{(s)} \ddot{Q}_2^{(p)}] - 2\Omega\alpha\dot{\phi}_x - 2\Omega \sum_{p=1}^{b} [\delta_p^{(s)} \dot{Q}_1^{(p)} + \gamma_p^{(s)} \dot{Q}_2^{(p)}] + k_{ux} u_s - k_{xy} \phi_y = 0$$

$$-\eta_n^{(s)} \ddot{u}_s + \xi_n^{(s)} \ddot{v}_s + A_n^{(s)} \ddot{\phi}_x + B_n^{(s)} \ddot{\phi}_y + \sum_{p=1}^{b} [Z_{n,p}^{(ss)} \ddot{Q}_1^{(p)} - Z_{n,p}^{(sc)} \ddot{Q}_2^{(p)}] - 2\Omega\gamma_n^{(s)} \dot{\phi}_x + 2\Omega\delta_n^{(s)} \dot{\phi}_y + 2\Omega \sum_{p=1}^{b} [(\alpha_{n,p}^{(ss)} - Z_{n,p}^{(sc)}) \dot{Q}_1^{(p)} - (Z_{n,p}^{(ss)} + \alpha_{n,p}^{(sc)}) \dot{Q}_2^{(p)}] + \Omega^2 \sum_{p=1}^{b} [(\beta_{n,p}^{(ss)} + \gamma_{n,p}^{(ss)} - Z_{n,p}^{(ss)} - 2\alpha_{n,p}^{(sc)}) Q_1^{(p)} + (Z_{n,p}^{(sc)} - \beta_{n,p}^{(sc)} - \gamma_{n,p}^{(sc)} - 2\alpha_{n,p}^{(ss)}) Q_2^{(p)}] + K_n^{(s)} Q_1^{(n)} = 0 \qquad \text{for } n = 1,2,\ldots,b$$

$$\xi_n^{(s)} \ddot{u}_s + \eta_n^{(s)} \ddot{v}_s + B_n^{(s)} \ddot{\phi}_x - A_n^{(s)} \ddot{\phi}_y + \sum_{p=1}^{b} [Z_{n,p}^{(sc)} \ddot{Q}_1^{(p)} + Z_{n,p}^{(ss)} \ddot{Q}_2^{(p)}] + 2\Omega\delta_n^{(s)} \dot{\phi}_x + 2\Omega\gamma_n^{(s)} \dot{\phi}_y + 2\Omega \sum_{p=1}^{b} [(Z_{n,p}^{(ss)} + \alpha_{n,p}^{(sc)}) \dot{Q}_1^{(p)} + (\alpha_{n,p}^{(ss)} - Z_{n,p}^{(sc)}) \dot{Q}_2^{(p)}] + \Omega^2 \sum_{p=1}^{b} [(2\alpha_{n,p}^{(ss)} - Z_{n,p}^{(sc)} + \beta_{n,p}^{(sc)} + \gamma_{n,p}^{(sc)}) Q_1^{(p)} + (\beta_{n,p}^{(ss)} + \gamma_{n,p}^{(ss)} - Z_{n,p}^{(ss)} - 2\alpha_{n,p}^{(sc)}) Q_2^{(p)}] + K_n^{(c)} Q_2^{(n)} = 0 \qquad \text{for } n = 1,2,\ldots,b$$

The constant coefficients which appear in these equations are defined in the following equations, where Σ_j implies summation over the azimuth, $j = 1,2\ldots$, number of blades, Σ_k implies summation over the node mass points within the finite element mesh, and Σ_r (Σ_s) imply summation over radial (tangential) beams used to account for centrifugal stiffening calculations.

$$\xi_n^{(s)} \triangleq \frac{N}{2} \sum_k \{(\mathrm{R}u_n^{(s)} - \mathrm{I}v_n^{(s)}) m\}_k$$

$$\eta_n^{(s)} \triangleq \frac{N}{2} \sum_k \{(\mathrm{R}v_n^{(s)} + \mathrm{I}u_n^{(s)}) m\}_k$$

$$\delta_n^{(s)} \triangleq \frac{N}{2} \sum_k \{(Q_1 \mathrm{R}w_n^{(s)} - Q_2 \mathrm{I}w_n^{(s)}) m\}_k$$

$$\gamma_n^{(s)} \triangleq \frac{N}{2} \sum_k \{(Q_1 \mathrm{I}w_n^{(s)} + Q_2 \mathrm{R}w_n^{(s)}) m\}_k$$

$$\lambda_n^{(s)} \triangleq \frac{N}{2} \sum_k \{Q_3 (\mathrm{R}u_n^{(s)} - \mathrm{I}v_n^{(s)}) m\}_k$$

$$\chi_n^{(s)} \triangleq \frac{N}{2} \sum_k \{Q_3 (\mathrm{I}u_n^{(s)} + \mathrm{R}v_n^{(s)}) m\}_k$$

Here R and I imply the real and imaginary parts, respectively.

$$A_n^{(s)} \triangleq \delta_n^{(s)} - \lambda_n^{(s)}, \qquad B_n^{(s)} \triangleq \gamma_n^{(s)} - \chi_n^{(s)}$$

$$C_n^{(s)} \triangleq \delta_n^{(s)} + \lambda_n^{(s)}, \qquad D_n^{(s)} \triangleq \gamma_n^{(s)} + \chi_n^{(s)}$$

$$F \triangleq \sum_j \sum_k m_{jk}, \qquad G \triangleq \sum_j \sum_k (Q_3 m)_{jk}$$

$$H \triangleq \frac{N}{2} \sum_k [\{(Q_1^2 + Q_2^2) + 2Q_3^2\} m]_k$$

$$\alpha = \frac{N}{2} \sum_k [(Q_1^2 + Q_2^2) m]_k$$

$$\sum_j \sum_k \{(u_p^{(s)} v_n^{(s)} - u_n^{(s)} v_p^{(s)}) m\}_{jk} \triangleq \alpha_{n,p}^{(ss)}$$

$$\sum_j \sum_k \{(u_p^{(c)} v_n^{(s)} - u_n^{(s)} v_p^{(c)}) m\}_{jk} \triangleq \alpha_{n,p}^{(sc)}$$

$$\sum_j \sum_k \{(u_p^{(s)} v_n^{(c)} - u_n^{(c)} v_p^{(s)}) m\}_{jk} \triangleq \alpha_{n,p}^{(cs)}$$

$$\sum_j \sum_k \{(u_p^{(c)} v_c^{(c)} - u_c^{(c)} v_p^{(c)}) m\}_{jk} \triangleq \alpha_{n,p}^{(cc)}$$

$$-\sum_j \sum_k \{(u_p^{(s)} u_n^{(s)} + v_p^{(s)} v_n^{(s)}) m\}_{jk} \triangleq \beta_{n,p}^{(ss)}$$

$$-\sum_j \sum_k \{(u_p^{(c)} u_n^{(s)} + v_p^{(c)} v_n^{(s)}) m\}_{jk} \triangleq \beta_{n,p}^{(sc)}$$

$$-\sum_j \sum_k \{(u_p^{(s)} u_n^{(c)} + v_p^{(s)} v_n^{(c)}) m\}_{jk} \triangleq \beta_{n,p}^{(cs)}$$

$$-\sum_j \sum_k \{(u_p^{(c)} u_n^{(c)} + v_p^{(c)} v_n^{(c)}) m\}_{jk} \triangleq \beta_{n,p}^{(cc)}$$

$$\sum_j \sum_k \{(u_p^{(s)} u_n^{(s)} + v_p^{(s)} v_n^{(s)} + w_p^{(s)} w_n^{(s)}) m\}_{jk} \triangleq Z_{n,p}^{(ss)}$$

$$\sum_j \sum_k \{(u_p^{(c)} u_n^{(s)} + v_p^{(c)} v_n^{(s)} + w_p^{(c)} w_n^{(s)}) m\}_{jk} \triangleq Z_{n,p}^{(sc)}$$

$$\sum_j \sum_k \{(u_p^{(s)} u_n^{(c)} + v_p^{(s)} v_n^{(c)} + w_p^{(s)} w_n^{(c)}) m\}_{jk} \triangleq Z_{n,p}^{(cs)}$$

$$\sum_j \sum_k \{ (u_p^{(c)} u_n^{(c)} + v_p^{(c)} v_n^{(c)} + w_p^{(c)} w_n^{(c)}) m \}_{jk} \triangleq Z_{n,p}^{(cc)}$$

$$\gamma_{n,p}^{(ss)} \triangleq \sum_j \sum_r \sum_s \left[m \left(Q_2 \int_{y_0}^{Q_2} \left[\frac{\partial w_p^{(s)}}{\partial y} \frac{\partial w_n^{(s)}}{\partial y} + \frac{\partial u_p^{(s)}}{\partial y} \frac{\partial u_n^{(s)}}{\partial y} \right] dy + Q_1 \int_{x_0}^{Q_1} \left[\frac{\partial w_p^{(s)}}{\partial x} \frac{\partial w_n^{(s)}}{\partial x} + \frac{\partial v_p^{(s)}}{\partial x} \frac{\partial v_n^{(s)}}{\partial x} \right] dx \right) \right]_{rsj}$$

$$\gamma_{n,p}^{(sc)} \triangleq \sum_j \sum_r \sum_s \left[m \left(Q_2 \int_{y_0}^{Q_2} \left[\frac{\partial w_p^{(c)}}{\partial y} \frac{\partial w_n^{(s)}}{\partial y} + \frac{\partial u_p^{(c)}}{\partial y} \frac{\partial u_n^{(s)}}{\partial y} \right] dy + Q_1 \int_{x_0}^{Q_1} \left[\frac{\partial w_p^{(c)}}{\partial x} \frac{\partial w_n^{(s)}}{\partial x} + \frac{\partial v_p^{(c)}}{\partial x} \frac{\partial v_n^{(s)}}{\partial x} \right] dx \right) \right]_{rs}$$

$$\gamma_{n,p}^{(cs)} \triangleq \sum_j \sum_r \sum_s \left[m \left(Q_2 \int_{y_0}^{Q_2} \left[\frac{\partial w_p^{(s)}}{\partial y} \frac{\partial w_n^{(c)}}{\partial y} + \frac{\partial u_p^{(s)}}{\partial y} \frac{\partial u_n^{(c)}}{\partial y} \right] dy + Q_1 \int_{x_0}^{Q_1} \left[\frac{\partial w_p^{(s)}}{\partial x} \frac{\partial w_n^{(c)}}{\partial x} + \frac{\partial v_p^{(s)}}{\partial x} \frac{\partial v_n^{(c)}}{\partial x} \right] dx \right) \right]_{rs}$$

$$\gamma_{n,p}^{(cc)} \triangleq \sum_j \sum_r \sum_s \left[m \left(Q_2 \int_{y_0}^{Q_2} \left[\frac{\partial w_p^{(c)}}{\partial y} \frac{\partial w_n^{(c)}}{\partial y} + \frac{\partial u_p^{(c)}}{\partial y} \frac{\partial u_n^{(c)}}{\partial y} \right] dy + Q_1 \int_{x_0}^{Q_1} \left[\frac{\partial w_p^{(c)}}{\partial x} \frac{\partial w_n^{(c)}}{\partial x} + \frac{\partial u_p^{(c)}}{\partial x} \frac{\partial u_n^{(c)}}{\partial x} \right] dx \right) \right]_{rs}$$

$$K_n^{(s)} \triangleq (w^{(n)})^2 M_n^{(s)} = (w^{(n)})^2 \sum_j \sum_k [\{ (u_n^{(s)})^2 + (v_n^{(s)})^2 + (w_n^{(s)})^2 \} m]_{jk}$$

$$K_n^{(c)} \triangleq (w^{(n)})^2 M_n^{(c)} = (w^{(n)})^2 \sum_j \sum_k [\{ (u_n^{(c)})^2 + (v_n^{(c)})^2 + (w_n^{(c)})^2 \} m]_{jk}$$

Acknowledgments

The research leading to this paper was supported by NASA Lewis Research Center under Grant NAG 3-37, Dr. R. Kielb, Technical Monitor. The authors also profited from discussions with Dr. J. Kiraly of NASA Lewis, Prof. E. Crawley of M.I.T., and C. Platt of Pratt & Whitney Aircraft Group, Commercial Products Division, UTC. Prof. M. Shephard of RPI provided invaluable help in computational aspects.

References

[1] Houbolt, J. C. and Anderson, R. A., "Calculation of Uncoupled Modes and Frequencies in Bending or Torsion of Nonuniform Beams," NACA TN 1522, 1948.

[2] Mendelson, A. and Gendler, S., "Analytical Determination of Coupled Bending-Torsion Vibrations of Cantilever Beams by Means of Station Functions," NACA TN 2185, 1950.

[3] Rosard, D. D., "Natural Frequencies of Twisted Cantilever Beams," *Journal of Appied Mechanics*, Vol. 20, 1953, pp. 241-244.

[4] Jarret, G. W. and Warner, P. C., "The Vibration of Rotating Tapered-Twisted Beams," *Journal of Applied Mechanics*, Vol. 20, 1953, pp. 381-389.

[5] Yntema, R. T., "Simplified Procedures and Charts for the Rapid Estimation of Bending Frequencies of Rotating Beams," NACA Rept. 3459, 1955.

[6] Houbolt, J. C. and Brooks, G. W., "Differential Equations of Motion for Combined Flapwise Bending, Chordwise Bending and Torsion of Twisted Nonuniform Rotor Blades," NACA Rept. 1346, 1958.

[7] Carnegie, W., "Vibration of Pretwisted Cantilever Blading," *Proceedings oif the Institution of Mechanical Engineers*, Vol. 173, 1959, pp. 343-362.

[8] Carnegie, W., "Vibrations of Rotating Cantilever Blading: Theoretical Approaches to the Frequency Problem Based on Energy Methods," *Journal of Mechanical Engineering Science*, Vol. 1, 1959, pp. 235-240.

[9] Isakson, G. and Eisley, J. G., "Natural Frequencies in Bending of Twisted Rotating Blades," NASA TN D-371, 1960.

[10] Steenivasamurthy, S. and Ramamurti, V., "A Parametric Study of Vibration of Rotating Pre-Twisted and Tapered Low Aspect Ratio Cantilever Plates," *Journal of Sound and Vibration*, Vol. 86, No. 3, 1981, pp. 311-328.

[11] Dokanish, M. A. and Rawtani, S., "Vibration Analysis of Rotating Cantilever Plates," *International Journal for Numerical Methods in Engineering*, Vol. 3, 1971, pp. 233-248.

[12] Petricone, R. and Sisto, F., "Vibration Characteristics of Low Aspect Ratio Compressor Blades," *Journal of Engineering for Power*, Vol. 93, 1971, pp. 103-110.

[13] Ahmed, S., Anderson, R. G., and Zienkiewicz, O. C., "Vibration of Thick Curved Shells with Particular Reference to Turbine Blades," *Journal of Strain Analysis*, Vol. 5, 1970, pp. 200-206.

[14] Bossak, M.A.J. and Zienkiewicz, O. C., "Free Vibration of Initially Stressed Solids with Particular Reference to Centrifugal-Force Effects in Rotating Machinery," *Journal of Strain Analysis*, Vol. 8, 1973, pp. 245-252.

[15] Henry, R. and Lalanne, M., "Vibration Analysis of Rotating Compressor Blades," *Journal of Engineering for Industry*, Vol. 3, 1974, pp. 1028-1035.

[16] Filstrup, A. W., "Finite Element Analysis of a Gas Turbine Blade," Paper No. 74-WA/GT-11, presented at the Winter Annual Meeting of the American Society of Mechanical Engineers, Nov. 17-22, 1974..

[17] Trompette, P. and Lalanne, M., "Vibration Analysis of Rotating Turbine Blades," Paper No. 74-WA/DE-23, presented at the Winter Annual Meeting of the American Society of Mechanical Engineers, Design Engineering Division, Nov. 17-22, 1974.

[18] MacBain, J. C., "Vibratory Behavior of Twisted Cantilever Plates," *Journal of Aircraft*, Vol. 12, 1975, pp. 343-349.

[19] Thomas, J. and Mota Soares, C. A., "Dynamic Analysis of Rotating Turbine and Compressor Blading," Paper No. C 193/76, International Conference on Vibration in Rotating Machinery, Cambridge University, Sept. 9, 1976.

[20] Ramamurti, V. and Steenivasamurthy, S., "Dynamic Stress Analysis of Rotating Twisted and Tapered Blades," *Journal of Strain Analysis*, Vol. 15, 1980, pp. 117-126.

[21] Prohl, M. A., "A Method for Calculating Vibration Frequency and Stress of a Banded Group of Turbine Buckets," *Transactions of ASME*, Vol. 80, No. 1, 1958, pp. 169-180.

[22] Deak, A. L. and Baird, R. D., "A Procedure for Calculating the Packet Frequencies of Steam Turbine Exhaust Blades," *Transactions of ASME*, Ser. A, Vol. 89, 1967, pp. 324-330.

[23] Carta, F. O., "Coupled Bladed-Disk-Shroud Flutter Instabilities in Turbojet Engine Rotors," *Journal of Engineering for Power, Transactions of ASME*, Vol. 89, 1967, pp. 419-426.

[24] Ewins, D. J., "Vibration Characteristics of Bladed Disk Assemblies," *Journal of Mechanical Engineering Science*, Vol. 15, No. 4, 1973, pp. 165-186.

[25] Mikolajczak, A. A., Arnoldi, R. A., Snyder, L. E., and Staragardter, H., "Advances in Fan and Compressor Blade Flutter Analysis and Predictions," *Journal of Aircraft*, Vol. 10, No. 4, 1975, pp. 325-332.

[26] Salama, A. L. and Petzt, M., "Dynamic Response of Packets of Blades by Finite Element Method," Paper 77-DET-70, presented at the Design Engineering Technical Conference, Chicago, Sept. 1977.

[27] Dugundji, J., "Flutter Analysis of a Tuned Rotor with Rigid and Flexible Disks," M.I.T., Cambridge, Mass., GT and PDL Report 146, July 1979.

[28] Fabunmi, J. A., "Forced Vibrations of a Single Stage Axial Compressor Rotor," ASME Paper 79-GT-108, presented at the Gas Turbine Conference, San Diego, Calif., 1979.

[29] Dugundji, J. and Chen, L.-T., "Investigation of the Vibration Characteristics of Shrouded Bladed Disk Rotor Stages," *Journal of Aircraft*, Vol. 17, July 1980, pp. 379-386.

[30] Wen-Hu Huang, "Free and Forced Vibration of Closely Coupled Turbomachinery Blades," *AIAA Journal*, Vol. 19, July 1981, pp. 918-924.

[31] Thomas, D. L., "Dynamics of Rotationally Periodic Structures," *International Journal for Numerical Methods in Engineering*, Vol. 14, 1979, pp. 81-102.

[32] Wildheim, J., "Vibrations of Rotating Circumferentially Periodic Structures," *Quarterly Journal of Mechanics and Applied Mathematics*, Vol. XXXIV, Pt. 2, 1981, pp. 213-229.

[33] Sisto, R. and Chang, A. T., "The Influence of Gyroscopic Forces on the Dynamic Behavior of Rotating Blades," The Fifth International Symposium on Air-Breathing Engines, Bangalore, India, Feb. 1981.

[34] Sisto, F., Chang, A. T., and Sutcu, M., "The Influence of Coriolis Forces on Gyroscopic Motion of Spinning Blades," presented at the 27th International Gas Turbine Conference and Exhibit, London, England, April 1982, *Journal of Engineering for Power*, Vol. 105, April 1983.

[35] Coleman, R. P., "Theory of Self-Excited Mechanical Oscillations of Hinged Rotor Blades," NACA ARR 3G29, July 1943.

[36] Scanlon, R. H. and Truman, J. C., "The Gyroscopic Effects of a Rigid Rotating Propeller on Engine and Wing Vibration Modes," *Journal of the Aerospace Sciences*, Vol. 17, Oct. 1950, pp. 653-659.

[37] Houbolt, J. C. and Reed, W. H., III, "Propeller-Nacelle Whirl Flutter," IAS Paper 61-34, presented at the 29th Annual Meeting, Jan. 1961.

[38] Crandall, S. H. and Dugundji, J., "Resonant Whirling of Aircraft Propeller-Engine Systems," *Journal of Applied Mechanics*, Dec. 1981, Vol. 48, pp. 929-935.

[39] Kaza, K.R.V. and Kvaternik, R. G., "Nonlinear Flap-Lag-Axial Equations of a Rotating Beam," *AIAA Journal*, Vol. 15, June 1977, pp. 871-874.

[40] Khader, N., "Structural Dynamics Analysis for Turbomachinery Bladed Disks," Ph.D. Thesis, Rensselaer Polytechnic Institute, Troy, N.Y., 1982.

[41] Loewy, R. G. and Khader, N., "Natural Frequency Prediction of Rotating Beams Using Non-Rotating Modes," *Journal of the American Helicopter Society*, Vol. 27, No. 2, April 1982, pp. 75-78.